Application of spatial cross correlation to detection of migration of submarine sand dunes

Garret P. Duffy and John E. Hughes-Clarke
Ocean Mapping Group, University of New Brunswick, Fredericton, New Brunswick, Canada

Received 22 June 2004; revised 4 March 2005; accepted 25 August 2005; published 12 October 2005.

[1] Knowledge of migration rates of bedforms provides an indirect indication of the behavior of tidally averaged bottom currents, enables optimization of hydrographic survey frequency and may enable calculation of bedload transport rate. To measure bedform migration rate, we test the use of spatial correlation as a measurement method, which quantifies and locates a region of maximum similarity between two spatial variables. For the latter, we use consecutive eight-bit images of spatial gradient, derived from bathymetric digital terrain models, carrying out the correlation over this representation of the shape of the seabed rather than the bathymetric surface. The digital terrain models were compiled from six repeat multibeam surveys of a headland-associated bank near Saint John, New Brunswick, with a roughly 30-day interval. Vectors are drawn depicting the movement of a sand dune at time t_0 toward a point in the spatial correlation array at a later time, t_1. A number of different techniques of picking the end of the migration vector were used. The sinuosity of the dune crest at the scale of the correlation window has an impact on which migration vector is the better pick. Averaging of migration vectors from consecutive epochs diminishes random errors in the correlation picks using any single pair of images and creates a more accurate picture of the migration field. Migration rates and crest-relative migration directions vary substantially across the sand bank, reflecting the high gradients in bottom shear stress around the headland.

Citation: Duffy, G. P., and J. E. Hughes-Clarke (2005), Application of spatial cross correlation to detection of migration of submarine sand dunes, *J. Geophys. Res.*, *110*, F04S12, doi:10.1029/2004JF000192.

1. Introduction

[2] Digital terrain models (DTMs) compiled from high-density multibeam echosounder (MBES) soundings are currently the highest-resolution representations of the morphology of a given area of seafloor. Airborne sounding techniques, such as LIDAR, can be more efficient than MBES techniques in the time it takes to survey an area but the poor sounding density and large sounding footprint area result in DTMs that are lower in resolution than MBES DTMs. Also unlike multibeam, LIDAR is limited to surveying in shallow non-turbid water so areas where active sediment transport is taking place may not be surveyed using this technique.

[3] We conducted six multibeam surveys of a headland associated sand bank, or "banner bank," with the intention of measuring the rate of migration of the sand dunes on the bank (Figure 1). Obviously, the scale of detectable displacement is controlled by the justifiable resolution of the DTM. The latter depends on the multibeam sounding density which in turn depends on factors such as water depth, beam footprint area, across-track beam spacing, ping rate and vessel speed. The presence of static bodies within the study area, such as bedrock outcrops, helped confirm the precise registration of successive surveys and ensured that detected displacements are real and not artifacts. With such a data set, we were particularly interested in gaining knowledge of the mechanisms forming and maintaining the bank.

[4] More generally, measurements of the dynamic behavior of bedforms are of immediate relevance to hydrographers wishing to optimize repetitive survey frequency [*Le Bot et al.*, 2000] and have been used by workers to calibrate their mathematical models [*Besio et al.*, 2004; *Nemeth et al.*, 2004]. Knowledge of bedform migration rate can also be combined with parameters describing the shape, height and composition of bedforms to calculate bedload transport rate [*Hoekstra et al.*, 2004; *Ten Brinke et al.*, 1999; *Van den Berg*, 1987; *Van Lancker et al.*, 2004; *Wilbers and Ten Brinke*, 2003]. *Duffy et al.* [2005] compare the bedform associated bedload transport rates observed on this sand bank with predicted rates derived from observed depth-averaged currents.

[5] A number of different approaches to measuring sand dune migration have been taken over the years. *Langhorne* [1982] took a direct measurement approach, staked out a large sand wave on the Skerries Bank in Start Bay, Devon, and employed divers to make continual measurements of the sand wave morphology over many tidal cycles. *Dorst* [2004] applied principles of geodetic deformation analysis to networks of soundings in a hydrographic approach to determine the degree, type and statistical significance of

Copyright 2005 by the American Geophysical Union.
0148-0227/05/2004JF000192

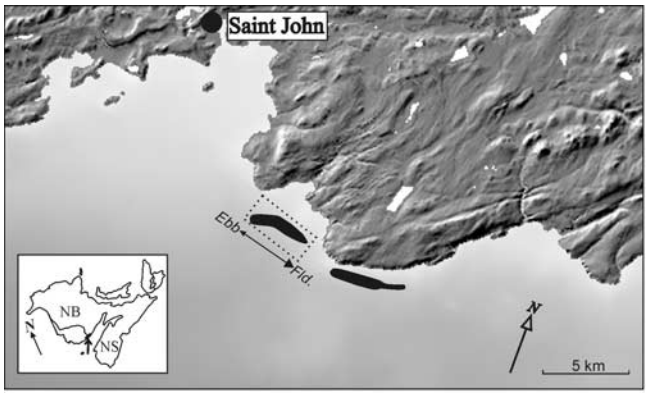

Figure 1. Overview map of the banner banks, defined by the black areas, and their relationship with the headland, Cape Spencer. The dotted square defines the bank under investigation in this study. The primary current directions over the sand bank are also shown with the larger arrow denoting dominant current direction.

seabed dynamics. *Lindenbergh* [2004] also took a geodetic deformation approach and used the model of a propagating sinusoidal wave which necessitated assumptions that dune spacing and celerity do not change in space. *Knaapen* [2004] observed the migration of bedforms through analysis of single beam soundings and multibeam data and measured migration by subtracting extracted crest lines and trough lines from multibeam data.

[6] How does one take advantage of the total coverage afforded by modern sonar techniques to detect change? One approach is simply to view the DTMs as frames in a movie and observe how the bedforms migrate [*Rubin*, 2000]. However, it is difficult and user-intensive to interpret and quantify the degree of migration especially if the bed configuration is complex and the study area is large.

[7] Since we are interested in detecting the change of a DTM from one period to another, we may subtract the DTMs and try to interpret the resulting isopach map to tell us how the crests of the bedforms changed. In Figure 2, two cross sections are displayed from the June and July surveys together with the difference between them. The arrows point out the positions of the crests at the different times. It is apparent that the difference cross section bears little quantitative information about the displacement of the crests. This method is more suited to assessing total volumetric change due to bedform migration. However, since such a volumetric method is based on subtracting absolute depth values at a point, the results are subject to motion related artifacts such as long period heave and tidal errors.

[8] In this paper, we propose to make full use of all the data in the DTM to determine how the bedforms have migrated with no a priori assumptions of dune spacing or spatial distribution of celerity. We do not look only at the displacement of the crest; such a measurement is limited in precision to the resolution of the DTM, which in turn is limited by the sounding footprint area. Furthermore, sand dunes may deform as they migrate so that the crest displacement may not necessarily equal the displacement of the center of mass of the dune [*Middleton and Southard*, 1984]. Instead, we pick a window of an image describing the shape of the DTM at time t_0 and try to find its best match at time t_1. The method described in this paper uses slope images as the data set and so is insensitive to long period heave and tidal errors.

[9] Discrete cross-correlation methods are widely used to analyze temporal, spatial, and spatiotemporal data series. Temporal cross correlation is used in seismic data processing to distinguish a known signal from noise [*Kearey and Brooks*, 1996]. Spatial cross correlation has been applied to pattern recognition in the motion picture industry [*Lewis*, 1995] and to image detection and registration in the remote sensing field [*Pratt*, 1991]. *Delacourt et al.* [2004] recently applied a digital cross-correlation technique to stereophotographs with the aim of measuring the three-dimensional displacement of a prominent landslide in south central France. In Particle Image Velocimetry, a cross-correlation technique is applied to a succession of digital images of a particle seeded flow to elucidate motion vectors [*Jambunathan et al.*, 1995; *Raffel et al.*, 1998; *Willert and Gharib*, 1991].

[10] This paper will concern itself with an application of a cross-correlation technique to consecutive DTMs of actively migrating sand dunes in Mispec Bay, Saint John, New Brunswick. Section 2 deals with the mathematics of cross correlation and its specific application in this research. Section 3 of this paper gives a background and description of the data sets used in this paper. Section 4 describes the results of different correlation pick types and the impact of morphology on migration measurement. Section 5 will be an interpretation of the migration vector field. Sections 6 and 7 are discussion and conclusion.

2. Theory and Implementation

[11] The spatial cross-correlation technique may be used to locate the point where two spatial data sets are most

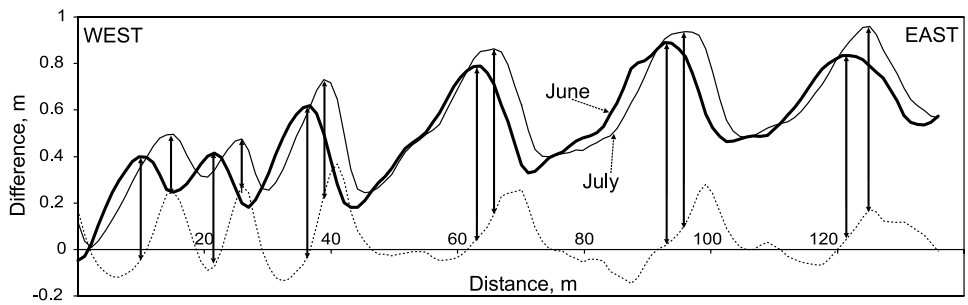

Figure 2. Depth cross sections and cross section through a difference DTM.

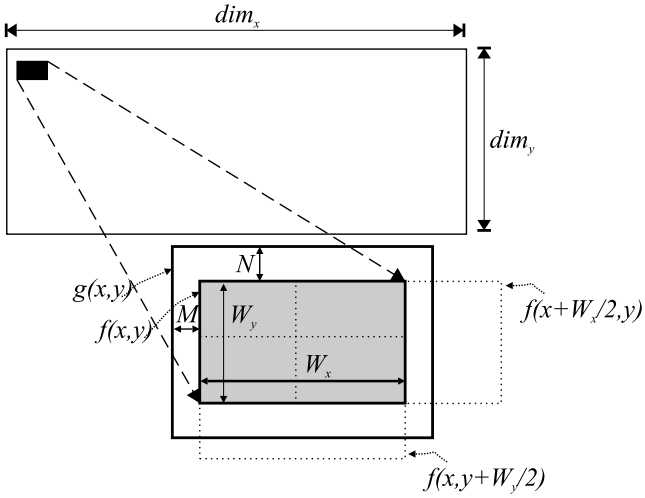

Figure 3. Diagram of *f*, *g*, and the data set.

similar. The cross-correlation coefficient quantifies the strength of correlation of two discrete data sets and is the sum of the products of overlapping pixels (equation (1), where $f(x, y)$ and $g(x, y)$ are windowed spatial variables with dimensions (W_x, W_y). The cross-correlation coefficient calculation is iterated by incrementing and decrementing the relative displacement in the x and y directions by k and l, respectively.

$$r_{k,l} = \sum_{x=0}^{W_x} \sum_{y=0}^{W_y} f(x,y) g(x-k, y-l),$$
$$-M \le k \le M, k \in Z, \quad -N \le l \le N, l \in Z,$$
$$r = \begin{bmatrix} r_{-M,N} & \cdots & \cdots & \cdots & r_{M,N} \\ \vdots & & & r_{k_{MAX},l_{MAX}} & \vdots \\ \vdots & & r_{0,0} & & \vdots \\ \vdots & & & & \vdots \\ r_{-M,-N} & \cdots & \cdots & \cdots & r_{M,-N} \end{bmatrix}. \quad (1)$$

[12] The position of the maximum of the resulting $2M+1$ by $2N+1$ matrix (M and N being the search parameters), (k_{MAX}, l_{MAX}), is the integer displacement of g relative to f where they are highest correlated. However two factors affect the effective implementation of equation (1): (1) bright spots or dark spots in g, for example, due to outlier soundings, will bias the maximum correlation value toward these areas so that a high r value may just reflect these anomalous spots; and (2) the magnitude of r is linked to the size of the window (W_x, W_y) so is not useful for comparisons with different window sizes. We therefore normalize r to R so that ($-1 \le R \le 1$) by subtracting the mean and dividing by the standard deviation (equation (2)).

$$R_{k,l} = \frac{\sum_{x=0}^{W_x} \sum_{y=0}^{W_y} \left[f(x,y) - \overline{f}\right] \left[g(x-k, y-l) - \bar{g}_{k,l}\right]}{\sqrt{\sum_{x=0}^{W_x} \sum_{y=0}^{W_y} \left[f(x,y) - \overline{f}\right]^2 \sum_{x=0}^{W_x} \sum_{y=0}^{W_y} \left[g(x-k, y-l) - \bar{g}_{k,l}\right]^2}}$$
$$-M \le k \le M, k \in Z, \quad -N \le l \le N, l \in Z. \quad (2)$$

Equation (2) is the expression used in this paper to calculate the correlation between f and g. Note how only the mean of g needs to be calculated at each lag value (k, l); the mean of f is independent of lag value since it is the pattern sought in g and need only be calculated once at the start of the iteration.

[13] Figure 3 illustrates the relationship between f, g and the entire data set dim_x by dim_y. Once the matrix of normalized cross-correlation R is fully populated, the windows f and g are advanced together to the next position in the data set. Figure 3 shows f at the next positions in the x and y directions by the dotted rectangles. In this case, there is 50% overlap of windows in both the x and y directions to ensure we have redundancy of measurement.

2.1. Selecting the Window Size and Search Parameter

[14] Some pre-analysis of the migration vector fields and the shape of the correlograms are necessary so that suitable values for the window size and search parameter can be chosen. Conceptually, the window size must be large enough so that it just encompasses a unique area of seafloor. If the window size is not large enough, then spurious displacement vectors will result. Therefore the window size must be chosen to be just large enough so that the number of outliers of migration vectors is minimized. The search parameter is chosen by examining a sample of correlograms taken throughout the field area as described in the following section.

2.2. Choosing the Migration Vector

[15] Up to this point the implementation of cross correlation is no different to that done in Particle Image Velocimetry (PIV) with one major exception: in PIV the fields of cross-correlated pixels are assumed to be random, therefore in the cross-correlation matrix there will be a circular point maximum to which a translation vector can be drawn.

[16] In the application of cross correlation discussed here, we are cross-correlating a linear feature with another linear feature that has been displaced. Depending on the sinuosity of this crest line, the resulting cross-correlation matrix will not have an obvious point maximum but an elliptical maximum or a correlation "ridge." This correlation morphology has important implications for the choice of migration vector as will be seen later.

[17] In Figure 4c, actual output resulting from cross correlating a 30 by 30 pixel subwindow is displayed. The following methods of measuring the displacement of the bedform were tested.

[18] 1. Method i involves taking the offset of the maximum correlation.

[19] 2. Method ii involves accounting for the shape of the cross-correlation peak by taking the weighted centroid (linearly weighted according to the ratio $R_{k,l}/R_{\max}$) of the part of the array greater than a certain threshold value, hereafter called the "threshold region." *Raffel et al.* [1998] describes this method in the context of PIV to be suitable for broad threshold regions with particle images less than 1.5 pixels in size. These criteria are met by the application of cross correlation presented here in which typical threshold regions are made up of 50 values (for search size of ±10 pixels) and the 'particles' in this case are equal to 1 pixel.

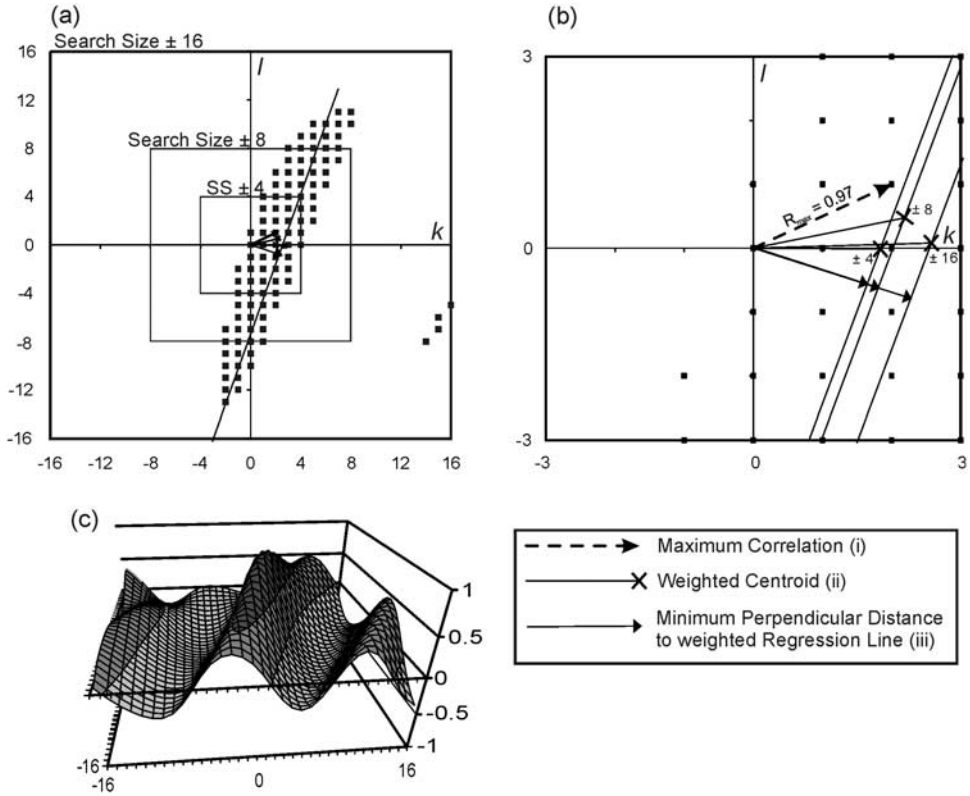

Figure 4. Different outputs of the spatial correlation algorithm using a 30 by 30 pixel (equals 30 by 30 m) window with search sizes of M, N = 4, 8, and 16 pixels. (a) Part of the cross-correlation array where $R_{k,l}$ is greater than the threshold value; the concentric rectangles show what part of the cross-correlation array is captured with the different search sizes. (b) A close-up view of the different cross-correlation picks at the different search sizes. Note the erratic centroid pick as the threshold region becomes more populated with each increment of search size and note the static maximum correlation pick. Also shown are the weighted regression lines calculated as the search size is incremented and shown are the minimum perpendicular distance points to those lines. (c) Shape of the variogram.

[20] 3. Method iii involves taking account of the spatial trend of the cross-correlation peak by calculating a weighted line of best fit on the points making up the threshold region and then locating the point on the line which is closest to the zero lag position. This forces the migration vector to have an orientation normal to the average orientation of matching crest lines at the different times; that is, in the event of no change in orientation of the crest lines, the migration vector will be perpendicular to the crest line. This is an acceptable assumption for 2-D dunes in a uniform flow field since it is widely accepted that in such a situation the dune crests lie perpendicular and migrate parallel to the net sediment transport direction [*Belderson*, 1982; *Rubin and Hunter*, 1987].

[21] The function of the threshold region is to define the shape of the base of the cross-correlation maximum. The authors found that a threshold value equal to the maximum correlation value divided by $\sqrt{2}$ satisfactorily described the plan view of correlation peak. The implications for this choice will be discussed later.

[22] An important advantage of using methods ii or iii is that displacements finer than the pixel size of the data sets may be resolved, unlike the maximum displacement, method i, which is constrained to integer displacements in the x and y directions. This is because we can consider the cross-correlogram, R, as a discretized continuous correlation surface and the actual peak of this function lies between the pixels [*Sjödahl*, 1994]. For this reason, method i is limited in accuracy and precision. Method ii is a method of interpolating for the true correlation peak. Method iii is a new method proposed by the authors and is specific to the cross correlation of linear features in that emphasis is given to the linear trend of the cross correlogram in addition to the correlation magnitude.

[23] Figures 4a and 4b illustrate the different methods to elucidate a migration vector. It is immediately evident that methods ii and iii are sensitive to different degrees on the number of points in the threshold region. This number depends on both the threshold value and the search size (see the concentric squares in Figure 4a enclosing different threshold regions for different search sizes). The centroid picks are erratic in azimuth and magnitude up until the threshold region is fully populated (represented by the black squares in the figure). Any wider searching is not needed because either it will not increase the number of points in the threshold region or it could detrimentally incorporate high correlation points from a proximal crest thereby getting a false lock (four such outliers at a search size greater than

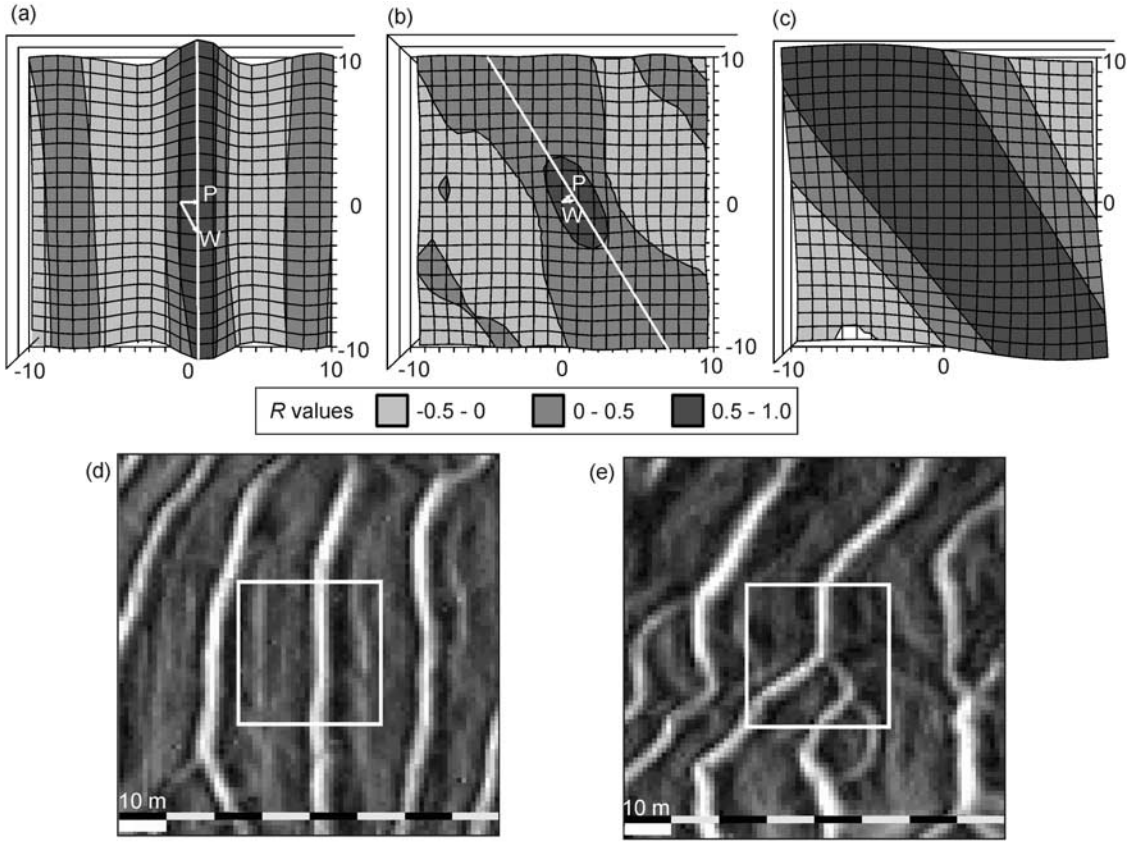

Figure 5. Different correlation morphologies of (a) a straight crested dune, using maximum slope of surface as the data type; (b) a bifurcating dune, using maximum slope of surface as the data type; and (c) the same bifurcating sand dune, using depth as the data type. The slopes of the (d) straight crested dune and (e) bifurcating dune are also shown with the correlation window outlined in white. P and W denote perpendicular regression and weighted centroid vectors, respectively.

±14 pixels are depicted in the lower right quadrant of Figure 4a). To minimize such spatial aliasing errors, the code was modified to only carry out the centroiding operation on the correlation ridge that is closest to the zero displacement position. The implication of the latter is that our survey frequency is such that spatial aliasing is not a problem: the bedforms have not migrated greater than half their spacing in the survey interval and the relevant correlation ridge is therefore the one closest to the origin.

[24] However, even if the threshold region is fully populated and the migration vector based on the weighted centroid method is stable, it is readily seen that a change in the threshold value can again cause the azimuth and magnitude of the vector to vary especially if the crest line has low sinuosity at the scale of the correlation window. In this latter case, high R values (greater than 90% of the maximum correlation value) can persist along the crest line at time t_2, affecting the position of the weighted centroid since the threshold region is not well-defined (Figure 5a shows the correlogram resulting in this case). It is clear that describing the migration of a straight-crested sand dune by fixing on its morphology (as the weighted centroid method does) is ambiguous and sensitive to input parameters. The linear regression method (method iii) surmounts this latter problem of unstable azimuths by making the assumption that migration is perpendicular to the crests. This assumption of crest-perpendicular migration is a fair one only if competent currents are uniform along the crest [*Dietrich and Smith*, 1984; *Rubin and Hunter*, 1985, 1987]. Current measurement cycles conducted over the sand bank have revealed that uniform currents over the 2-D dunes flow 80% of the tidal cycle toward the headland [*Duffy et al.*, 2004] so we are confident that these straight crested dunes migrate perpendicular to their crests. Migration vectors arising from this method are in general less subject to variation in magnitude than vectors calculated from the centroid method and their azimuth is already fixed. However, they are insensitive to marked crest-oblique migration.

[25] For dunes with three-dimensional features such as sinuosity, bifurcations or terminations in the window of interest, the locus of such high R values is an enclosed ellipse rather than a line. Figure 5b shows the shape of the correlation function for sand dune with a bifurcation. In this case the centroid method is a more reliable indicator of displacement since there is a better-defined peak to which a stable vector may be drawn.

[26] To summarize, the weighted centroid vector method may be used in all cases except where there are straight crested dunes, then the perpendicular method is more suitable.

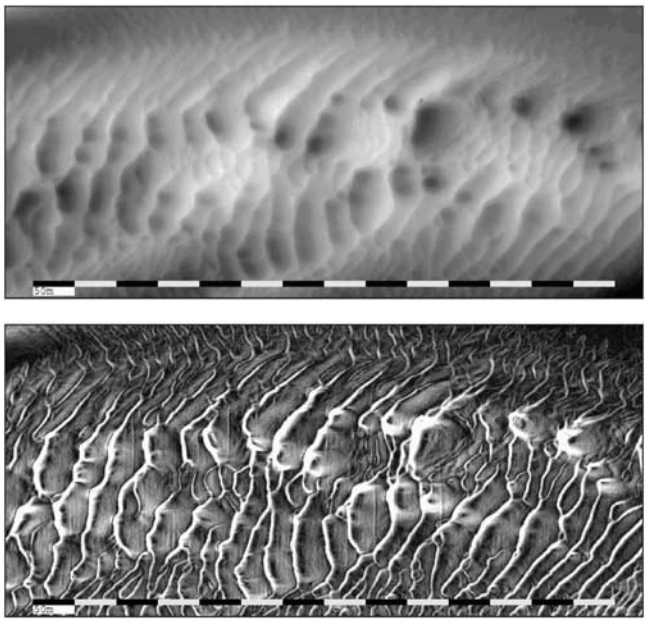

Figure 6. Different representations of the seafloor. (top) Eight-bit digitized depth showing slowly varying pixel values on the sand dunes. (bottom) Spatial gradient of bathymetry emphasizing dune morphology.

2.3. Data Preprocessing

[27] The type of representation of the bathymetric surface is of paramount importance to the detection of migration of bedforms. The cross-correlation algorithm works best when the input data contains regions of rapidly varying pixel shade. However, the features of interest, bedforms, are characterized by large areas of slowly changing depth (Figure 6 (top)). If we carry out the cross correlation on this representation of the bathymetric surface, then we get very broad correlogram in which the centroid or regression vector pick would be unreliable (Figure 5c). Clearly, this data type does not help us do the job of picking where the crests of the dunes are most highly correlated. Using software developed by Ocean Mapping Group, *addSUN*, we experimented with various representations of the DTM morphology. We found that sun-illuminated representations emphasized dune morphology satisfactorily although we found that the resulting migration vector was dependent on the azimuth of the virtual Sun. The "-omni" option in "addSUN" generates an image of the slope of the DTM at a point; this data type showed no change in migration vector since there were no extra parameters in the slope calculation, such as azimuth or elevation of a virtual Sun.

[28] We have therefore used this image showing the maximum slope at a pixel to emphasize the dune morphology (Figure 6, bottom). The correlogram of the dune using this data type (Figure 5b), shows how much better defined the correlation peak is when using the slope data as input.

[29] When we make this slope image, we lose any depth information of the data set. This is acceptable since the focus of this paper is the horizontal migration of the sand dunes, not the vertical change due to accretion or deflation. Inspection of depth cross sections showed that vertical shifts in bathymetry not due to migration of the dunes were at the limit of the vertical accuracy of the data set owing to datum and tidal issues and therefore difficult to quantify.

3. Data Acquisition and Description

[30] Six consecutive Simrad EM-3000 multibeam surveys of dynamic sand dunes in Mispec Bay, Saint John, New Brunswick were carried out from April to September in 2002 using the Ocean Mapping Group's vessel *C.S.L. Heron*. The EM-3000 measures depths with equiangular beam spacing port and starboard so the sounding density and footprint area are strongly nadir biased. To counteract this, survey lines were run with a constant spacing of 30 m so that the dense nadir soundings of one line overlapped the lower density soundings of the previous line thus increasing the overall sounding density.

[31] In terms of survey resolution, the footprint area of each sounding places a limit on the resolution of the individual sounding. As can be seen in Table 1 a single nadir sounding is returned for a circular area of diameter of roughly 80 cm in 30 m of water and 100 cm in 40 m of water [*Hare*, 1995] (this depth range defines the sand bank). This is satisfactory resolution for studying the bedforms in this area that have larger dimensions than this resolution (the smallest spacing of dunes resolved in 40 m depth is 10 m) [*Hughes-Clarke*, 1998]. The quantity of interest for producing an accurate DTM is the sounding density and this has been measured to approximately 2.7 m^{-2} thanks to the considerable overlap between lines (Table 1). These repeat measurements of the same patch of seafloor also average out random errors making our horizontal measurement of position of a bin more accurate. As evinced by apparent displacement of the bedrock described later, there is still of course the possibility that positional uncertainty can cause outliers in the DTM. However, since we are cross correlating a 30 by 30 pixel window, we are confident that such random errors will not affect the position of the maximum correlation, rather it may cause a decrease in the maximum cross correlation. Another GPS related error is positional bias due to multipath but this has a correlation time ($\sim$1 min) less than the period of the next observation of a given area

Table 1. Geometrical Parameters of the Simrad EM-3000, Which Has 127 Beams With a Nadir Beam Width of 1.5° by 1.5°[a]

	Depth 30 m	Depth 40 m
Vessel speed over ground, knots	9	9
Ping rate, Hz	4	4
Soundings along track at nadir, m^{-1}	0.8	0.8
Soundings across track at nadir, m^{-1}	2.5	1.3
Soundings across track at 45°, m^{-1}	1.8	0.6
Beam footprint area at nadir, m^2	0.5	0.9
Beam footprint area at 45°, m^2	1.9	3.4
Average number of soundings, 100% coverage, m^{-2}	1.4	1.1
Average number of soundings, actual coverage, m^{-2}	2.8	2.7

[a]Depths depicted are typical of the sand bank. The beam footprints are spaced within a swath so that they overlap each other across track by 50%. The values in the penultimate row of the table are the number of soundings per square meter if there was no overlap between the lines. Surveys were conducted in this research with 250% coverage in the deeper water and 200% coverage in the shallow water because of the dependence of swath width on water depth.

Table 2. Dates of Multibeam Surveys With Intervals

Date	Interval Between Surveys, days
24 April 2002	...
18 May 2002	24
30 June 2002	43
1 August 2002	32
27 August 2002	26
2 October 2002	36

of seafloor (~15 min, the time between lines) so this error is effectively randomized and its effect is minimized. Considering first of all the sounding density, sonar resolution and worst possible DGPS error, we decided on a grid resolution of 1 m^2/pixel.

[32] The Canadian Hydrographic Service–operated tide gauge at Saint John was used for tidal reduction of soundings. Analysis of cross lines revealed that extrapolation of the tide to the field area 10 km away caused a vertical error of 5–10 cm, or 0.3% water depth, which is well within specification for this sonar. Vessel attitude and heading were given by a variety of instruments for different surveys such as POS-MV 320, Seapath 200 RTK, Seatex MRU-6 and a Meridian Gyrocompass. Sound speed in the water column was measured using an AML conductivity temperature and depth sensor mounted in a Brook Ocean Technology towbody.

[33] The field area encloses a 3 km by 1 km "banner bank," one of a pair of such banks situated either side of the nearby headland, Cape Spencer (Figure 1). The depth of the top of the sand bank ranges from 22 m below chart datum in the center of the bank close to the headland to 40 m below chart datum around the seaward periphery. The tide range is on average 6.5 m (neaps: 5 m; springs: 8.5 m).

[34] The sand bank is characterized by dunes that gradually increase in dimension from heights and spacings of 0.2 m and 10 m, respectively, in the deeper parts to 2.5 m and 40 m where the sand bank rises to 25 m depth. The large dunes have a marked asymmetry indicating net migration eastward toward the headland (Figure 2 illustrates the asymmetry of some typical dunes).

[35] Three ADCP tidal current measurement cycles reveal that the currents just inshore of the sand bank are strongly unidirectional, with currents flowing 80% of the time toward the headland in the flood direction [*Duffy et al.*, 2004]. The long duration of currents flowing in this direction is due to the clockwise ebb tidal eddy that contributes currents toward the headland in addition to flood currents. The swiftest currents (measured to be ~110 cm/s (depth averaged)) and most dynamic bedforms are confined to a broad (100 m wide), 2.5 m deep negative topographic feature that demarcates the landward part of the sand bank adjacent to the headland (Area B, Figure 8). Such a channel has also been noted on another banner bank adjacent to Portland Bill, U.K. [*Bastos et al.*, 2002; *Dyer and Huntley*, 1999] albeit in that case the channel was much deeper (~100 m) since it took advantage of a contrast in geology at that point.

[36] The tidal regime around Saint John harbor and the Bay of Fundy as a whole is dominated by the M2 tidal constituent because of the resonant effect of the natural frequency of the Bay with this tidal constituent [*Greenberg*, 1979; *Sankaranarayanan and McCay*, 2003]. *Besio et al.* [2004] claimed that even small M4/M2 ratios could cause upstream migration due to mode superposition effects but even then upstream migration was strongly affected by the phase relationship between these components. *Besio et al.* [2004] does not go into detail about the lower limit of |M4|/|M2| necessary to induce upstream migration but states that a value of 0.072 may cause upstream migration if the necessary phase relationship exists. In nearby Saint John harbor, the |M4|/|M2| ratio is 0.017 [*Sankaranarayanan and McCay*, 2003] so we believe we can make the assumption that the morphology and dune activity is strongly linked to the tidally averaged current field.

[37] The active nature of the sand dunes on the bank was discovered through inspection of four Geological Survey of Canada cruises conducted at six monthly intervals in 2000 and 2001. Although the slow moving dunes could be tracked over the 6-month interval, the fast moving dunes could not be tracked with confidence since their migration rate was greater than half of their spacing per sample period. Therefore a more frequent interval was chosen to capture the movement of these fast moving dunes (Table 2 gives the intervals between the surveys) with the duration of a single survey lasting 7 hours.

[38] To rule out possible measured dune displacements due to dune crest oscillations over a tidal cycle such as those noted by direct measurements of a sand dune conducted by *Langhorne* [1982], a separate hydrographic survey of a small area of the sand bank was carried out during an M2 tidal cycle in October 2002 in which the same area of seafloor was passed over every 30 min. No dune migration within the resolution of the instrument was noted over this survey so we can make the necessary assumption that detected migration is due to tidally integrated sediment transport rather than short-term crest oscillations.

[39] Bedrock outcrops in the area confirmed proper registration of the monthly DTMs. Maximum apparent displacements of these outcrops were of the order of 1.5 m; this was observed for the April–May interval, thereafter apparent displacements were not resolvable on the 1-m DTM.

4. Results

[40] Pre-analysis was first carried out to determine optimal window and search sizes. Optimum window size was sought by trial and error. A small window size caused spurious vectors since the windows did not contain a unique portion of the seafloor. A square window size of side 30 pixels (equal to 30 m for this DTM) produced the most uniform vector field over the entire sand bank. We assume that a series of small dunes that fall within a single large window do not move independently over such a short length scale. Their migration may therefore be described by a single vector.

[41] Selecting search size was not so straightforward for reasons outlined in section 2.2. In the case of vectors calculated by the centroid and linear regression methods, their directions and azimuths were dependent on search size up until the elliptical threshold region was fully populated, found to be on average ±10 pixels, as described in Figure 4.

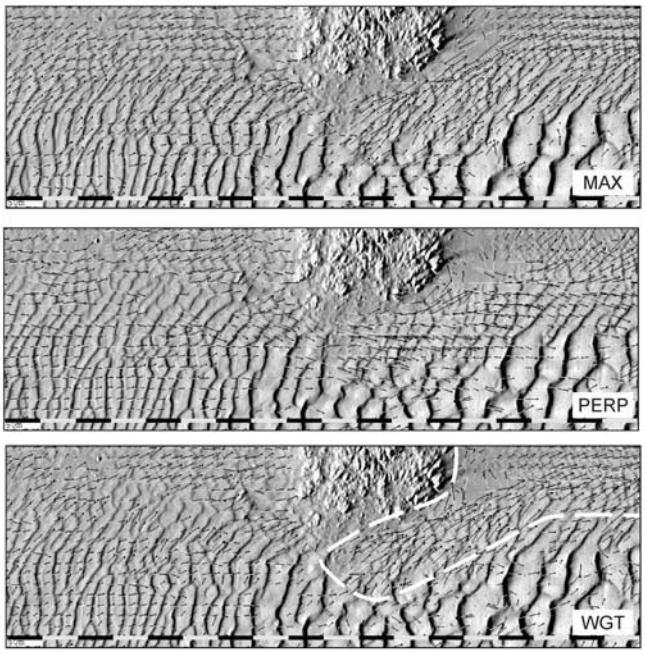

Figure 7. Different correlation picks on the dunes for a window size of 30 by 30 and search size of ±10. Vectors are averaged from the five vector fields. (top) Picking the maximum correlation (method i); (middle) Picking the minimum perpendicular distance to the regression line (method iii). (bottom) Picking the weighted centroid (method ii).

However, as Figure 5a shows, even with such a search size the centroid vectors in the case of straight crested dunes will not be stable.

[42] For the fore-going reasons, experimentation with different correlation pick types was done with a window size of 30 pixels and a search parameter of ±10 pixels.

4.1. Experimenting With Different Correlation Pick Types

[43] In Figure 7, monthly averaged outputs for running the algorithm with the three different options (maximum correlation (method i), threshold region line of best fit (method iii) and weighted centroid (method ii) are shown. For ease of explanation in the text, the order of method ii and method iii have been reversed.

4.1.1. Maximum Correlation (Method i)

[44] This vector field for the most part overestimated the migration rate (Figure 7 (top)). As outlined by *Sjödahl* [1994] and *Raffel et al.* [1998], it makes little sense to use this vector type since the vector is constrained to integer pixel displacements in the x and y directions. In addition, since the threshold region may be quite broad and a well-defined sharp peak does not exist, statistically it makes more sense to take into account the shape of the threshold region when calculating the migration vectors.

4.1.2. Regression Line of Correlation Array (Method iii)

[45] These vectors were almost everywhere perpendicular to the crest lines, since they were forced to be so by the minimum perpendicular distance to the regression line of the threshold region condition. Vector subtraction of the regression line vectors from the weighted centroid vectors demonstrated that in regions of the sand bank with three-dimensional dunes, only in one area were the weighted centroid vectors systematically different from the regression vectors; this indicates that crest oblique migration was happening. In the regions of straight crested dunes, there was some random difference between the regression vectors and weighted centroid vectors for reasons outlined in section 2.2.

4.1.3. Correlation Array Weighted Centroid (Method ii)

[46] As stated, vector subtraction between regression and centroid vector revealed the presence of crest oblique migration. This area is outlined with the white dashed line in Figure 7. Bedforms that were migrating perpendicular to their crests and parallel to the sediment transport direction migrate into this region where the current suddenly changes in direction and magnitude, because of acceleration around the bedrock obstacle. This induces the sediment transport direction to change across a distance too short for the bedforms to adjust as they migrate, causing crest-oblique migration. This phenomenon has been postulated for submarine dunes by *Rubin* [1998], observed in river meanders by *Dietrich and Smith* [1984] and in sub-aerial dunes by *Rubin and Hunter* [1985].

[47] The fact that in this region the bedforms are sinuous and in some cases terminate in the window makes the weighted centroid more trustworthy in this situation as described in section 2.2.

4.2. Migration Velocities

[48] To calculate migration rates, the calculated displacement vectors were converted to average migration velocities (in m/month, where 1 month = 30 days) by taking account of the survey interval (Table 2). Assuming that the separate migration velocity fields were in effect 5 different observations of the same phenomenon, they were then temporally averaged together to produce a more coherent vector field describing the migration regime of the sand bank. This averaging process reduced the prominence of spurious migration vectors in featureless seafloor while maintaining the true migration vector field.

[49] We can remove outliers from the averaged vector field by removing all vectors at a certain point that have a standard deviation of azimuth greater than a certain amount. This method was useful for removing noisy vectors that had erratic azimuths in each of the five vector fields. In this work, we filtered out vectors that had standard deviations of azimuth of greater than 60°. This resulted in the elimination of most of the vectors in the featureless seabed and vectors where there was negligible movement.

4.3. Migration Vector Precision and Accuracy

[50] We used DGPS positioning which gave our horizontal position to within 1.5 m at 95% level of accuracy, as quoted by the manufacturer. A number of stages of averaging in the processing of migration vectors make them more accurate.

[51] 1. The compilation of the DTM by binning the soundings into a 1-m grid averages out the horizontal errors

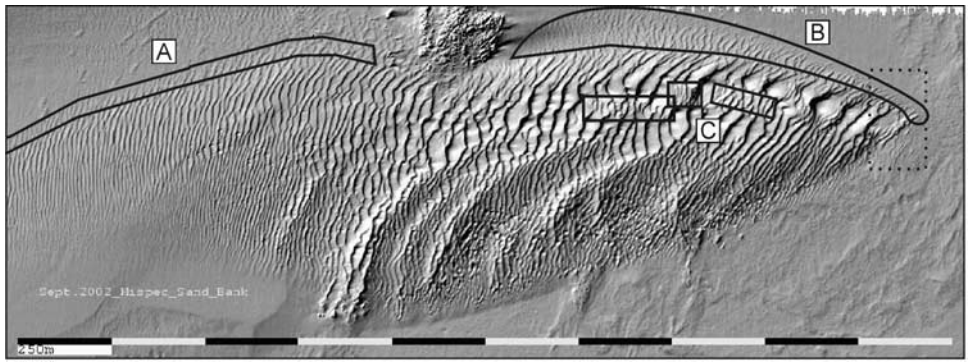

Figure 8. Overview of the sand bank with the areas of most active migration outlined in black. The dotted rectangle is the location of Figure 9.

of the soundings within that bin, making the averaged horizontal position of the averaged sounding more accurate. The fact that some of the soundings in a single bin are from different survey lines at different times helps minimize bias errors due to multipath.

[52] 2. Since we are quantizing the DTM into 30 m by 30 m units, outliers in horizontal position within this large window have less of an impact as described in section 3. In addition, this window size encompasses multibeam soundings from multiple opposing survey lines along which biases are unlikely to be correlated.

[53] 3. Considering the vector field as a whole, overlapping successive correlation windows in the x and y direction increases the ''signal to noise'' ratio of the vector field by increasing the redundancy of displacement measurement.

[54] 4. Since each vector field is based on only two observations of state of the sand bank, stacking the migration vectors considerably increases their accuracy. Filtering based on standard deviations of azimuth and magnitude helps eliminate vectors in areas where no migration is occurring.

[55] To find out which of the correlation pick methods were most accurate in terms of migration magnitude we measured the 2D Cartesian displacement of a sample of dunes throughout the sand bank from the April survey to the September survey and taking into account the interval, calculated their average migration rate between those two periods. The precision of this ''eye-balling'' of the Cartesian migration rate is one pixel from the April survey to the September survey which translates to 0.20 m/month.

[56] We found that whereas the azimuth of the weighted centroid vector could vary with the threshold value, its magnitude and the magnitude of the regression vectors were very close to the Cartesian migration rate, both being within ±0.40 m/month of the Cartesian rate. The technique successfully resolved average migration rates down to 0.8 m/month.

5. Interpretation

[57] As pointed out in the introduction, the underlying justification of this method of development was to better understand sediment transport processes of the banner bank. To that end, the following pertinent observations could now be made as a result of this method.

[58] Inspection of the migration vector field of this banner bank reveals substantial spatial variability of movement. Overall, the dunes of spacing 20 m are the most active with mean and peak migration rates of 3.0 and 4.5 m/month respectively in area B (Figure 8). Note that these bedforms are only 30 cm in height; this shows the power of using the DTM slope data, rather than bathymetry, in this instance. The most active of these dunes occur where the sand bank laterally peters out to featureless seabed to the north (area A in the figure); in the base of the channel that delimits the north-western part of the sand bank (area B); and at a number of flat patches in the sand bank where the depth is shallower than 27 m below mean water level (areas C). The larger (50 m spacing, 3 m high) dunes on the sand bank proper migrate slower with average migration rates of 0.9–1.1 m/month.

[59] We theorize that the increase in the net bedload transport to landward in areas A and B cause the lateral increase in migration velocities. Sediment sampling has indicated that that seafloor landward of the sand bank is composed of bimodal medium sand and gravel whereas the sand bank itself is composed of moderately well sorted medium sand and fine sand [*Duffy et al.*, 2004]. Therefore we propose that immediately landward of areas A and B the net bedload transport is high enough to winnow away the sand, washing away the 30-cm-high bedforms and forming the bimodal lag deposit. Area B also has locally increased dominant current due to the channelized nature of the flow here.

[60] Where the sand bank comes to a narrow ''tip'' close to the headland, there is evidence of bedforms becoming barchanoid in planform before being obliterated as the peak dominant current moves into the upper plane bed field (Figure 9); this is characteristic of increasing bottom shear stress toward the headland and could be evidence of a ''bedload parting zone'' surrounding the headland as described by *Kenyon et al.* [1981]. Such a bedload parting zone has been hypothesized to exist in the vicinity of another headland, Portland Bill, UK, by *Bastos et al.* [2002] on the basis of surficial geology and current modeling.

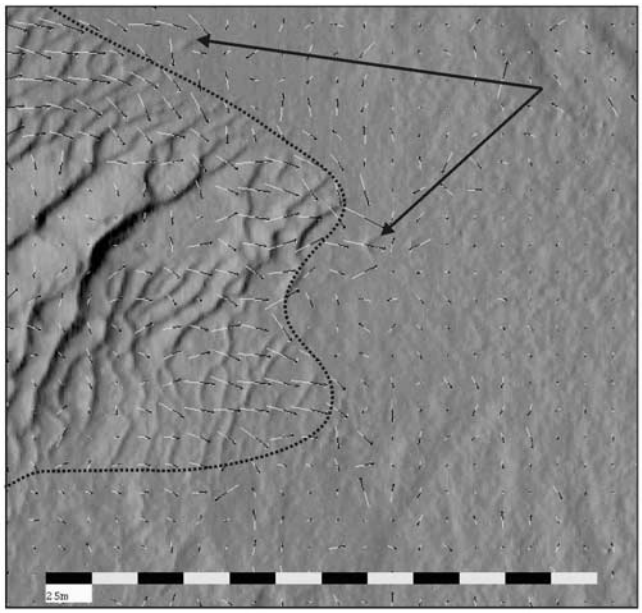

Figure 9. Picture showing accelerated migration of bed forms in two lobes at the tip. The weighted centroid vectors in these areas indicate migration rates of up to 3 m/month. The sand bank is demarcated by the dotted line. The arrows point out some examples of barchanoid dunes found in Area B.

[61] The relative elevation of area C implies that sediment transport rates will be higher at this point because of increased wave action; hence the swiftly migrating bedforms.

6. Discussion

[62] From examining the results, we can make the following statements.

[63] 1. Both perpendicular regression and weighted centroid methods of picking the end of the migration vector are accurate to within ±0.5 pixel per month. Table 3 summarizes vector applicability to dune type. The crest perpendicular vectors must be used in the event of straight crested dunes because the centroid pick, which depends on the existence of a unique trackable feature, cannot be used in this case. However, the crest-perpendicular migration assumption is only valid for uniform competent flow conditions. Indeed, as noted by *Rubin and Hunter* [1987], without knowledge of the current field, it is impossible to determine migration directions of straight crested dunes from remotely sensed images. The centroid pick must be used in all other cases, for example, sinuous dunes, bifurcating dunes or dune crests that terminate in the correlation window so that oblique migration, if present, may be detected. Inspection of the linearity of the correlograms is therefore necessary to decide which one of the two vectors is representative. This latter step has been recently automated by making the selection of centroid or regression vector be dependant on the ratio of the long axis to the short axis of the threshold region.

[64] 2. Since a correlation vector is based on a threshold region, and describes a region of "best-fit" between successive images of (the slope of) a dune, it better reflects the horizontal translation of the volume of a sand dune rather than a method which relies purely on the translation of a dune crest. This is especially true of dunes which have deformed after their migration, as noted by *Middleton and Southard* [1984] and observed by *Langhorne* [1982].

[65] 3. Treating the five month-to-month vector fields of translation as separate observations of the same phenomenon enables "stacking" of the vectors to produce vectors of migration rate. This enables us to get a clearer and more accurate picture of the average migration regime on the sand bank than a single observation.

[66] 4. The more observations of the sand bank done, the better the accuracy of the migration vectors providing the frequency of surveying is such so that spatial aliasing of sand dunes is avoided. This means that the survey frequency must be high enough so that sand dunes with the highest ratio of spacing to migration rate do not migrate more than half their spacing in the survey interval. For instance, the small dunes in the western part of the sand bank have a spacing of 12 m and average migration rates of 2 m/month. This means that to avoid aliasing, the survey period must be shorter than 3 months.

[67] 5. In this paper, we used a Simrad EM-3000 multibeam with a 1.5° by 1.5° nadir beamwidth. The use of a higher-resolution multibeam, such as the Reson Seabat 8125 with a nadir beamwidth of 0.5° by 1.0°, would of course enable finer detail to be resolved which would enable the tracking of smaller scale features such as ripples climbing on the backs of larger dunes. If migration is to be detected at this scale, high-precision horizontal positioning such as RTK-GPS becomes necessary and the vessel's speed must be decreased to ensure high along-track sounding density. There is also the possibility that crest oscillations that may occur over a tidal cycle could be detected. The vector field output for the motion of the dunes described in this paper should not be different with a higher-resolution sonar. Any difference could be due to tidal crest oscillations resolved by the higher-resolution multibeam.

7. Conclusion

[68] The technique described in this paper successfully reproduced a credible migration vector field on a sand bank through analysis of successive slope images compiled from dense, high-resolution multibeam sounding data. The migration of even small (30 cm high) dunes was resolved since the data input into the algorithm described the slope not absolute depth and the survey frequency was high enough so that the fastest moving bedforms had not moved greater than half their spacing during the survey interval (i.e., aliasing was not an issue). We found the assumption of crest perpendicular migration to be invalid in the part of the

Table 3. Summary Table of Migration Vector Applicability to Dune Morphology and Crest-Relative Migration Direction

Dune Type	3-D, Crest Perpendicular	3-D, Crest Oblique	2-D, Crest Perpendicular	2-D, Crest Oblique
Regression vector	Y	N	Y	N
Weighted centroid vector	Y	Y	N	N

sand bank down current of a bedrock obstacle where non-uniform currents are experienced but valid in the region of straight crested dunes in the interior of the sand bank where currents are uniform.

[69] **Acknowledgments.** The authors wish to thank Carmen Reid, Howard Ingalls and Loren Fleet for their skilled piloting of *Heron*. The authors also wish to thank Anya Duxfield for her tireless field support. The authors are grateful to the sponsors of the Chair of Ocean Mapping Group (University of New Brunswick) and the National Seabed Survey of Ireland for financial support.

References

Bastos, A., N. H. Kenyon, and M. Collins (2002), Sedimentary processes, bedforms and facies, associated with a costal headland: Portland Bill, Southern U.K., *Mar. Geol.*, *187*, 235–258.

Belderson, R. H. (1982), Bedforms, in *Offshore Tidal Sands: Processes and Deposits*, edited by A. H. Stride, pp. 27–55, CRC Press, Boca Raton, Fla.

Besio, G., P. Blondeaux, M. Brocchini, and G. Vittori (2004), On the modeling of sand wave migration, *J. Geophys. Res.*, *109*, C04018, doi:10.1029/2002JC001622.

Delacourt, C., P. Allemand, B. Casson, and H. Vadon (2004), Velocity field of the "La Clapiere" landslide measured by the correlation of aerial and QuickBird satellite images, *Geophys. Res. Lett.*, *31*, L15619, doi:10.1029/2004GL020193.

Dietrich, W. E., and J. D. Smith (1984), Bed load transport in a river meander, *Water Resour. Res.*, *20*(10), 1355–1380.

Dorst, L. L. (2004), Geodetic deformation analysis: A new method of the estimation of seabed dynamics, in *Marine Sandwave and River Dune Dynamics II, International Workshop*, edited by S. J. M. H. Hulscher, T. Garlan, and D. Idier, pp. 64–71, Univ. of Twente, Enschede, Netherlands.

Duffy, G. P., J. E. Hughes-Clarke, and R. Parrott (2004), Application of current measurement and time lapsed bathymetric multibeam surveying to investigation of a banner bank, Mispec Bay, New Brunswick, Canada, in *Marine Sandwave Dynamics and River Dune Dynamics II, International Workshop*, edited by S. J. M. H. Hulscher, T. Garlan, and D. Idier, pp. 72–79, Univ. of Twente, Enschede, Netherlands.

Duffy, G. P., J. E. Hughes-Clarke, and D. R. Parrott (2005), Bedforms and associated sand transport on a banner bank, Saint John, NB, paper presented at Geological Association of Canada, Mineral. Assoc. of Can., Halifax, N. S., Canada.

Dyer, K. R., and D. A. Huntley (1999), The origin, classification and modelling of sand banks and ridges, *Cont. Shelf Res.*, *19*, 1285–1330.

Greenberg, D. A. (1979), A numerical model investigation of tidal phenomena in the Bay of Fundy and Gulf of Maine, *Mar. Geod.*, *2*, 161–187.

Hare, R. (1995), Depth and positioning error budgets for multibeam echosounding, *Int. Hydrogr. Rev.*, *72*(2), 37–69.

Hoekstra, P., P. Bell, P. van Santen, N. Roode, F. Levoy, and R. Whitehouse (2004), Bedform migration and bedload transport on an intertidal shoal, *Cont. Shelf Res.*, *24*, 1249–1269.

Hughes-Clarke, J. E. (1998), The effect of fine scale seabed morphology and texture on the fidelity of swath bathymetric sounding data, paper presented at Canadian Hydrographic Conference, Can. Hydrogr. Serv., Victoria, British Columbia, Canada.

Jambunathan, K., X. Y. Ju, B. N. Dobbins, and S. Ashforth-Frost (1995), An improved cross correlation technique for particle image velocimetry, *Meas. Sci. Technol.*, *6*, 507–514.

Kearey, P., and M. Brooks (1996), *An Introduction to Geophysical Exploration*, 2nd ed., Blackwell, Malden, Mass.

Kenyon, N. H., R. H. Belderson, A. H. Stride, and M. A. Johnson (1981), Offshore tidal sand banks as indicators of net sand transport and as potential deposits, *Spec. Publ. Int. Assoc. Sedimentol.*, *5*, 257–268.

Knaapen, M. A. F. (2004), Measuring sand wave migration in the field: Comparison of different data sources and an error analysis, in *Marine Sandwave Dynamics and River Dune Dynamics II, International Workshop*, edited by S. J. M. H. Hulscher, T. Garlan, and D. Idier, pp. 152–159, Univ. of Twente, Enschede, Netherlands.

Langhorne, D. N. (1982), A Study of the dynamics of a marine sandwave, *Sedimentology*, *29*, 571–594.

Le Bot, S., D. Idier, T. Garlan, A. Trentesaux, and D. Astruc (2000), Dune dynamics: From field measurements to numerical modeling—Application to bathymetric survey frequency in the Calais-Dover Strait, in *Marine Sandwave Dynamics*, edited by A. Trentesaux and T. Garlan, pp. 101–108, Univ. of Lille, Lille, France.

Lewis, J. P. (1995), Fast Template Matching, in *Vision Interface*, pp. 120–123, Can. Image Process. and Pattern Recognition Soc., Quebec.

Lindenbergh, R. (2004), Parameter estimation and deformation analysis of sand waves and mega ripples, in *Marine Sandwave Dynamics and River Dune Dynamics II, International Workshop*, edited by S. J. M. H. Hulscher, T. Garlan, and D. Idier, pp. 192–199, Univ. of Twente, Enschede, Netherlands.

Middleton, G. V., and J. B. Southard (1984), Mechanics of sediment movement, *SEPM Short Course*, *3*, 401 pp.

Nemeth, A. A., S. J. M. H. Hulscher, and R. M. J. Van Damme (2004), Modelling sand wave migration and height, comparing model results and data, in *Marine Sandwave Dynamics and River Dune Dynamics II, International Workshop*, edited by S. J. M. H. Hulscher, T. Garlan, and D. Idier, p. 352, Univ. of Twente, Enschede, Netherlands.

Pratt, W. K. (1991), *Digital Image Processing*, 2nd ed., John Wiley, Hoboken, N. J.

Raffel, M., C. E. Willert, and J. Kompenhans (1998), *Particle Image Velocimetry, a Practical Guide*, Springer-Verlag, New York.

Rubin, D. M. (1998), *Cross-Bedding, Bedforms, and Paleocurrents*, Soc. for Sed. Geol. (SEPM), Tulsa, Okla.

Rubin, D. M. (2000), Time-lapse movies of migrating bedforms, in *Marine Sandwave Dynamics, International Workshop*, edited by A. Trentesaux and T. Garlan, p. 177, Univ. of Lille, Lille, France.

Rubin, D. M., and R. E. Hunter (1985), Why deposits of longitudinal dunes are rarely recognised in the geologic record, *Sedimentology*, *32*, 147–157.

Rubin, D. M., and R. E. Hunter (1987), Bedform alignment in directionally varying flows, *Science*, *237*, 276–278.

Sankaranarayanan, S., and D. F. McCay (2003), Three-dimensional modeling of tidal circulation in Bay of Fundy, *J. Waterway Port Coastal Ocean Eng.*, *129*(3), 114–123.

Sjödahl, M. (1994), Electronic speckle photography: Increased accuracy by nonintegral pixel shifting, *Appl. Opt.*, *33*(28), 6667–6673.

Ten Brinke, W. B. M., A. W. E. Wilbers, and C. Wesseling (1999), Dune growth, decay and migration rates during a large-magnitude flood at a sand and mixed sand-gravel bed in the Dutch Rhine River system, *Spec. Publ. Int. Assoc. Sedimentol.*, *28*, 15–32.

Van den Berg, J. H. (1987), Bedform migration and bed-load transport in some rivers and tidal environments, *Sedimentology*, *34*, 681–698.

Van Lancker, V., J. Lanckneus, S. Hearn, P. Hoekstra, F. Levoy, J. Miles, G. Moerkerke, O. Monfort, and R. Whitehouse (2004), Coastal and nearshore morphology, bedforms and sediment transport pathways at Teignmouth (U.K.), *Cont. Shelf Res.*, *24*, 1171–1202.

Wilbers, A. W. E., and W. B. M. Ten Brinke (2003), The response of subaqueous dunes to floods in sand and gravel bed reaches of the Dutch Rhine, *Sedimentology*, *50*, 1013–1034.

Willert, C. E., and M. Gharib (1991), Digital particle image velocimetry, *Exp. Fluids*, *10*, 181–193.

G. P. Duffy and J. E. Hughes-Clarke, Ocean Mapping Group, University of New Brunswick, PO Box 4400, Fredericton, NB, Canada E3B 5A3. (garret@omg.unb.ca)